Luminescence imaging of photoelectron spin precession during drift in a p-type GaAs microfabricated Hall bar

V. Notot, D. Paget, A. Rowe, L. Martinelli, Fabian Cadiz, S. Arscott

Journal of Applied Physics

Luminescence imaging of photoelectron spin precession during drift in a p-type GaAs microfabricated Hall bar

Cite as: J. Appl. Phys. **121**, 125703 (2017); https://doi.org/10.1063/1.4979097
Submitted: 23 February 2017 • Accepted: 12 March 2017 • Published Online: 28 March 2017

V. Notot, D. Paget, A. C. H. Rowe, et al.

Luminescence imaging of photoelectron spin precession during drift in a p-type GaAs microfabricated Hall bar

V. Notot,[1] D. Paget,[1] A. C. H. Rowe,[1] L. Martinelli,[1] F. Cadiz,[2] and S. Arscott[3]
[1]*Physique de la matière condensée, Ecole Polytechnique, CNRS, Université Paris Saclay, 91128 Palaiseau, France*
[2]*Université de Toulouse, INSA-CNRS-UPS, 31077 Toulouse Cedex, France*
[3]*Institut d'Electronique, de Microélectronique et de Nanotechnologie (IEMN), University of Lille, CNRS, Avenue Poincaré, Cité Scientifique, 59652 Villeneuve d'Ascq, France*

(Received 23 February 2017; accepted 12 March 2017; published online 28 March 2017)

Using a microfabricated p-type GaAs Hall bar, it is shown that the combined application of coplanar electric and magnetic fields enables the observation of spatial oscillations of the photoluminescence circular polarization due to the precession of drifting spin-polarized photoelectrons. Observation of these oscillations as a function of electric field gives a direct measurement of the minority carrier drift mobility and reveals that the spin coherence length can be tuned up to more than 10μm with electric fields below 1 kV/cm. *Published by AIP Publishing.*
[http://dx.doi.org/10.1063/1.4979097]

I. INTRODUCTION

In the context of future active spintronic devices, the diffusion[1–3] and drift[4–9] of spins in semiconductors have been investigated by numerous authors. N-type GaAs seems particularly promising because of the weak spin relaxation,[10] but p-type material cannot be overlooked since in proposed bi-polar spintronic devices,[11] it is the minority carrier (electron) spin that determines the common base current gain. While in a p-type material charge transport has been widely investigated,[12–14] only a few studies have considered spin transport.[15,16] For all these studies, while time-resolved investigations give direct access to the transport dynamics, continuous wave (CW) imaging of spin transport, using luminescence,[17] or Kerr microscopy[1] gives diffusion and drift lengths from which it is possible to obtain spin mobilities provided that spin lifetimes are measured independently.[3]

In the present work, we investigate charge *and* spin transport in p-type GaAs using a CW photoluminescence (PL) imaging technique.[17] The photoelectrons are generated by a tightly focused circularly polarized laser excitation and acquire in the applied electric field $\vec{E}$ a drift velocity $\vec{v} = \mu_e \vec{E}$, where μ_e is the mobility. Their precession in the magnetic field B, applied in the sample plane, occurs with a frequency $\omega = \hbar^{-1} g^* \mu_B B$, where $g^* = -0.44$ is the effective Landé factor, $2\pi\hbar$ is Planck's constant, and μ_B is the Bohr magneton. This precession produces spatial oscillations of the component of the electronic polarization along the direction of excitation. By imaging the degree of circular polarization of the luminescence, one obtains the spatial period of these oscillations, approximately given by

$$l \approx \mu_e \frac{E}{B} \frac{h}{g^* \mu_B}. \quad (1)$$

The measurement of l directly gives the photoelectron drift mobility. This semi-quantitative picture neglects for simplicity the mechanisms for loss of spatial spin coherence, which are mostly due to diffusion and to spin relaxation, as characterized by the time T_1, and which introduce a damping of the oscillations and a possible slight shift of the extrema. Thus, precession in a magnetic field tranverse to the light excitation acts to effectively time-resolve the experiment and enables the measurement of the relevant parameters for spin transport. This method is analogous to investigations of spin precession using Kerr microscopy[18,19] and has the originality of using luminescence, thus giving access to spectroscopic investigations and to simultaneous measurements of charge and spin transport.

II. EXPERIMENTAL

As shown in Fig. 1, we use a Hall bar, microfabricated from a 3 μm-thick p-type GaAs sample (acceptor doping 10^{18} cm^{-3}) on a semi-insulating substrate. The electric field electric field is applied to the [110] crystallographic direction.[20] The maximum value of the electric field used here (800 V/cm) is well below that required to saturate the drift velocity at low temperatures.[21] A magnetic field of 0.23 T is permanently applied in the sample plane. A CW laser at 1.59 eV is tightly focused to a spot of gaussian half width $\sigma \approx 0.5$ μm, as measured from the spatial profile of the laser beam reflected from the sample surface. The excitation power is very low (12 μW), so that photoelectron transport is not affected by ambipolar effects[15,20] or by Pauli blockade.[16,22] The luminescence is focused on the entrance slit of the spectrometer, parallel to the longitudinal axis x of the Hall bar defined in the bottom panel of Fig. 1, and one monitors the image provided by a CCD camera placed in the output plane. All experiments are performed at a lattice temperature of ≈40 K.

For $E = 0$, an image of the PL intensity is shown in Panel a of Fig. 2. A cut of this image along its horizontal axis, perpendicular to the entrance slit, gives the local luminescence spectrum at a given distance r from the excitation spot. An example of such a spectrum at $r = 0$ is shown in

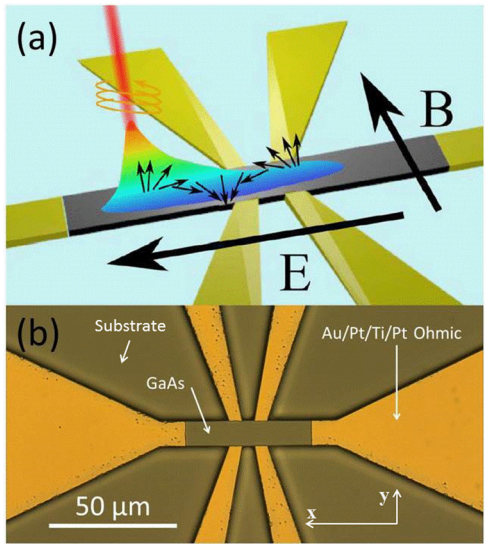

FIG. 1. Panel a shows the principle of the experiment. Photoelectrons are created by a circularly polarized tightly focussed light excitation in a Hall bar where an electric field is applied. The luminescence degree of circular polarization of photoelectrons drifting in this electric field is imaged. This imaging reveals the precession of the photoelectronic spins in a magnetic field applied in an arbitrary direction parallel to the sample plane. Panel b shows an optical microscopy image of the microfabricated Hall bar.

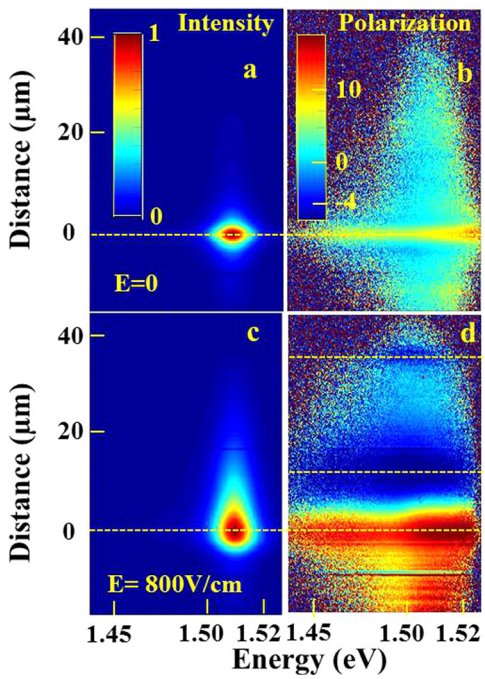

FIG. 2. Combined effects of electric and magnetic fields on the images detected by the CCD Camera at the output of the spectrometer. The temperature is 50 K and a magnetic field of 0.23 T is applied perpendicular to the excitation light direction. The vertical direction represents the distance on the sample to the excitation spot (along axis x shown in Fig. 1. Section of the images along the horizontal direction shows an intensity (panels a and c) and a circular polarization spectrum (Panels b and d) at the corresponding position at the sample surface. Panels a and c represent the intensity images for $E=0$ and $E=800$ V/cm and their comparison reveals the drift of the electrons in the electric field. Panels b and d represent the corresponding images of the luminescence degree of circular polarization and show the oscillations induced by precession during drift.

Curve a of the bottom panel of Fig. 3 and reveals, as expected for p^+ GaAs,[23] a single relatively broad emission line centered at 1.497 eV. From the exponential high energy tail of the spectrum, we obtain a photoelectron temperature of $T_e=48$ K. Conversely, a cut of the image along the vertical axis (parallel to the entrance slit) gives the spatial intensity profile at a given energy, along a line on the sample parallel to the spectrometer entrance slit and to the electric field (the origin of ordinates denoting the distance to the excitation spot). For $E=0$, this profile at the energy of the maximum of the PL intensity is shown in Curve a of the left panel of Fig. 4.

Panel c of Fig. 2 shows the corresponding image at $E=800$ V/cm. This image reveals a tail of drifting electrons extending over several tens of microns that is essentially independent of energy and is revealed from the spatial profile shown in Curve h of Fig. 4. The shape of the luminescence spectrum is independent of position, and this spectrum at the excitation spot and for $E=800$ V/cm is shown in Curve b of the bottom panel of Fig. 3. It is seen that the main effect of the electric field is to change the slope of the exponential tail, so that T_e is increased to $T_e\approx 60$ K.

Liquid crystal modulators are used to control the helicity of the excitation and to select the $\sigma^{\pm}$-polarized components of the luminescence, of intensity $I(\sigma^{\pm})$. It is then possible to monitor the difference signal $I_D=I(\sigma^+)-I(\sigma^-)$, in order to obtain the luminescence polarization image $\mathscr{P}=[I(\sigma^+)-I(\sigma^-)]/I$. This quantity is related to the spin density $s=n_+-n_-$, defined as the difference of

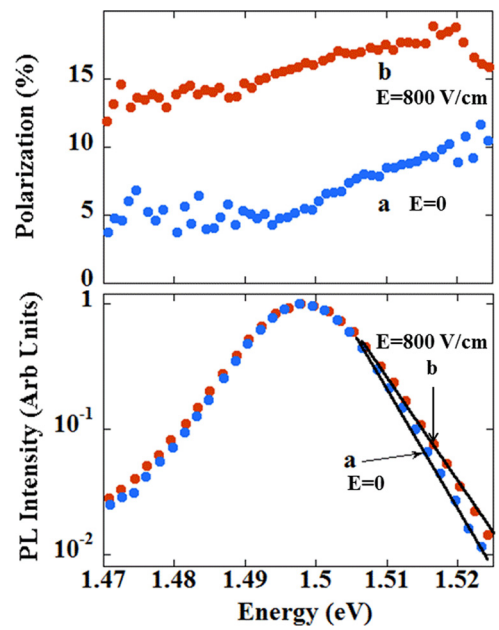

FIG. 3. The bottom panel shows cuts along the x direction of the images of panel a and panel b of Fig. 2 and exhibits the luminescence intensity spectra at the excitation spot for $E=0$ and $E=800$ V/cm (Curves a and b, respectively). The straight lines show that the high energy tails of these spectra can be approximated by exponentials, from which the temperature of the photoelectron gas can be obtained. The top panel shows, in the same conditions, the luminescence polarization spectra, obtained from cuts along the x direction of panels b and d, of Fig. 2, respectively. The decreased polarization at $E=0$ with respect to $E=800$ V/cm is caused by the larger dwell time at the excitation spot, which increases the magnitude of the Hanle effect.

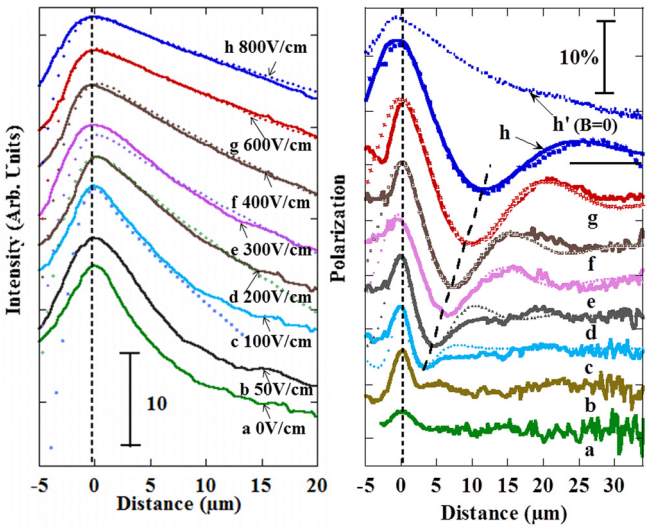

FIG. 4. The left panel shows the spatial profiles, shifted vertically for clarity, of the luminescence intensity for increasing values of the electric field and for a magnetic field $B = 0.23$ T. The right panel shows the polarization profiles in the same conditions. Spatial oscillations of the polarization due to electronic spin precession during drift appear for a field larger than 100 V/cm and, as expected from Eq. (1), their period increases with electric field. In contrast, as shown in Curve h' taken for $E = 800$ V/cm, no oscillations are observed for $B = 0$. Also shown by dotted lines in the two panels are calculations in the drift regime using parameter values given by Table I.

the concentrations of spins + and − with a quantization axis parallel to the excitation light direction, by $\mathscr{P} = |\mathscr{P}_i|s/(n_+ + n_-)$. Here, $|\mathscr{P}_i| = 0.5$ is the ratio between electron spin polarization and luminescence circular polarization. An image of $\mathscr{P}$ taken at $E = 0$ is shown in Panel b of Fig. 2. The luminescence polarization spectrum at the excitation spot is shown in Curve a of the top panel of Fig. 3.

Panel d of Fig. 2 shows the luminescence polarization image for $E = 800$ V/cm. The polarization at the excitation spot, as also shown by Curve b of the top panel of Fig. 3, is increased to about 15% since, because of the large photoelectron drift velocity, which reduces their effective lifetime at the excitation spot. Note also that the spectra shown in the top panel of Fig. 3 exhibit a lower degree of circular polarization on the high energy side of the line than on the low energy one. This effect, also observed here without any electric of magnetic field, can quite generally be caused by a difference in lifetimes or spin relaxation times[24,25] or by a change in the relevant hole states, resulting in a decrease of $|\mathscr{P}_i|$ for the low energy part of the line. However, no variation of lifetime or spin relaxation time can be found by time-resolved luminescence over the entire spectrum,[3] suggesting that the lower polarization is rather caused by a decrease of $|\mathscr{P}_i|$.

The key result of the present paper is the appearance of spatial oscillations. One observes regions of negative polarization, shown in Panel d of Fig. 2 by dashed lines at distances of 10 μm and 33 μm, separated by a positive extremum at a distance of 27 μm. The positions of the extrema weakly depend on energy in the spectrum. Fig. 4 shows the spatial profiles of the intensity (left panel) and polarization (right panel) at the energy (1.50 eV) of the maximum luminescence signal and for selected electric field values. The polarization oscillations are observed for an electric field larger than 50 V/cm and, as expected from Eq. (1), their spatial period increases with E. For lower electric fields (Curves a and b), the dominant transport process is spatially incoherent diffusion so that no oscillations are visible. In comparison, Curve h′ shows the polarization profile for $B = 0$ and $E = 800$ V/cm. As expected, no oscillations are visible and the polarization decays monotonically with distance because of spin relaxation during drift.

III. INTERPRETATION

A. Calculation of the polarization profiles

The photoelectron concentration in the steady-state is given by the drift-diffusion equation

$$0 = g(r,z) - \frac{n}{\tau} + \vec{\nabla}\left(\mu_e n\vec{E} + D\vec{\nabla}n\right), \tag{2}$$

where D is the diffusion constant of photoelectrons and τ is the photoelectron lifetime. The generation rate $g(r, z)$ depends on depth z and distance to the center of the excitation spot r according to $g(r,z) = \alpha g_0 \exp[-\alpha z - (r/\sigma)^2]$, where α is the light absorption coefficient, and σ is the gaussian half width of the excitation spot. Here $r = \sqrt{x^2 + y^2}$, where the corresponding axis is defined in panel b of Fig. 1. To calculate the spatial spin distribution, it is convenient to define the complex spin density $s_\pm = s_z \pm i s_Y$ where Y is the direction of the sample plane perpendicular to the orientation of the magnetic field, which can be arbitrary in the sample plane. The drift-diffusion-precession equation for $s_\pm$ is

$$g(r,z)\eta\mathscr{P}_i - \frac{s_\pm}{\tau_s}\left(1 \mp i\frac{B}{\Delta B}\right) + \vec{\nabla}\cdot\left[\mu_e\vec{E}s_\pm + D\vec{\nabla}s_\pm\right] = 0. \tag{3}$$

This equation is obtained from the charge equation by replacing $g(r, z)$ by $g(r,z)\eta\mathscr{P}_i$, where $\mathscr{P}_i$ is equal to ± 0.5 for $\sigma^{\mp}$-polarized light excitation and η accounts for polarization losses during thermalization. The time τ has been replaced by the complex spin lifetime $\tau_s/(1 \mp iB/\Delta B)$, where $\Delta B = \hbar/(g^*\mu_B\tau_s)$ is the Hanle linewidth. The spin lifetime τ_s is given by T_1 by $1/\tau_s = 1/\tau + 1/T_1$.

A solution of these equations for a film of thickness d is given in the Appendix, where the charge and spin density are decomposed into a series of modes, for each of which the z dependence is an eigenfunction of the Laplacian operator, satisfying the boundary conditions determined by the recombination velocities of the front and back surfaces, S and S', respectively. As discussed in the Appendix, it is reasonable at low temperature to consider only the spatial mode of lowest order, implying that, to first order in $Sd/D \ll 1$ and $S'd/D \ll 1$, the effect of surface recombination is mostly to replace τ by τ^* given by $1/\tau^* = 1/\tau + (S + S')/d$. The spatial dependence of the luminescence intensity after averaging over the sample thickness is given by

$$I(r) = A\frac{\alpha g_0 \tau e^{\beta x}}{2\pi}\left(\frac{\mathscr{L}_1}{L_d^*}\right)^2\left(K_0\left(\frac{|r|}{\mathscr{L}_1}\right) * e^{\left[-\left(\frac{r}{\sigma}\right)^2 + \beta x\right]}\right), \tag{4}$$

where A is a constant and K_0 is the modified Bessel function of the second kind, the operator * stands for two-dimensional convolution and the effective length $\mathscr{L}_1$ is given by

$$\frac{1}{\mathscr{L}_1} = \sqrt{\frac{1}{L_d^{*2}} + \beta^2}. \tag{5}$$

The effective charge diffusion length, taking into account surface recombination, is $L_d^* = \sqrt{D\tau^*}$. The inverse length β is given by

$$\beta = -\frac{\mu E}{2D} = -\frac{qE}{2k_B T_e}, \tag{6}$$

where q is the absolute value of the electronic charge and k_B is Boltzmann's constant. As shown by the right hand side of Eq. (6) where Einstein's relation has been applied, β only depends on E and on the temperature T_e of the photoelectron gas. At large charge drift distances x parallel to the electric field and in the charge drift regime defined by $\beta L_d^* \gg 1$, the profile described by Eq. (4) decays like $\exp[-x/(\mu E\tau^*)]$. The spatial profile of the polarization is given by

$$\mathscr{P}(r) = \eta \mathscr{P}_i^2 \frac{\tau_s\left(1+\beta^2 L_d^{*2}\right)}{\tau\left(1+\beta^2 L_s^{*2}\right)} \times Re\left\{\frac{K_0\left(\frac{|r|}{\mathscr{L}_1^s}\right) * e^{\left[-\left(\frac{r}{\sigma}\right)^2+\beta x\right]}}{(1\mp iB/\Delta B^*)\left(K_0\left(\frac{|r|}{\mathscr{L}_1}\right) * e^{\left[-\left(\frac{r}{\sigma}\right)^2+\beta x\right]}\right)}\right\}, \tag{7}$$

where $\Delta B^* = \Delta B(1+\beta^2 L_s^2)$, $L_s^* = \sqrt{D\tau_s^*}$ and $1/\tau_s^* = 1/\tau_s + (S+S')/(Dd)$, and $\mathscr{L}_{1s}$ is given by

$$\frac{1}{\mathscr{L}_{1s}} = \sqrt{\frac{1\mp iB/\Delta B}{L_s^{*2}} + \beta^2}. \tag{8}$$

Because $\mathscr{L}_1^s$ is complex, the function K_0 in the numerator of Eq. (7) has an oscillating spatial behavior. These oscillations are superimposed on a spatial polarization decay, which is described by $\exp[-x/(\mu E T_1)]$ at large distance and in the spin drift regime defined by $\beta L_d^* \gg 1$ and $\beta L_s^* \gg 1$.

B. Analysis of polarization spatial profiles

In the present section, we only consider the spatial profiles for $E > 50$ V/cm, i.e., in the drift regime where polarization oscillations are observed. Approximate values of the photoelectron mobilities are first determined from the positions of the extrema using Eq. (1) which is accurate to within about 10%. More accurate mobility values are obtained using a fit of Eq. (7) and the results only weakly depend on charge and spin lifetime values. These mobility values, given in Table I, strongly decrease with increasing electric field from 9000 cm^2/V s to about 4000 cm^2/V s. Shown in panel a of Fig. 5 is the dependence of the drift velocity $\mu_e E$ as a function of electric field. For electric fields lower than about 300 V/cm, the velocity is approximately proportional to the electric field, suggesting quasi ohmic transport. For higher fields, the velocity tends to saturate with a maximum value, of several 10^6 cm/s at 800 V/cm. This value is smaller than the usual saturation velocity by at least one order of magnitude.[21] This saturation is therefore not caused by the usual mechanisms usually invoked such as phonon or intervalley scattering, but by the heating of the electron gas which results in a decrease of the mobility.

TABLE I. Analysis of intensity and polarization profiles in the drift regime ($E > 50$ V/cm). Measured values of electronic temperature and polarization at the excitation spot, and values of electron mobility, $\eta\mathscr{P}_i^2$, and spin and charge lifetimes used in the adjustments of the curves in Fig. 4. Numbers in parentheses give the uncertainties of the determinations.

E (V/cm)	T_e (K) (K)	$\mathscr{P}(0)$ (%)	μ_e (cm^2/V s)	$\eta\mathscr{P}_i^2$ (%)	T_1 (ns)	τ^* (ns)	$\mu_e E T_1$ (μm)
100	49	6.4	9000	19	0.32(10)	0.33(5)	3.0
200	51	8.8	6800	13.7	0.50(10)	0.33(5)	7.0
300	52	9	6400	11.5	0.51(10)	0.33(5)	9.8
400	56	12.6	5000	14	0.47(10)	0.33(5)	9.4
600	58	14.8	4400	15	0.47(10)	0.33(5)	12.4
800	60	16.4	4200	17	0.33(10)	0.33(5)	11

In order to interpret this result, it should be pointed out that application of the electric field may perturb the Boltzmann nature of the distribution, as suggested by the Boltzmann equation formalism[26] and observed for high-purity material.[27] Here, as shown in Fig. 5, this perturbation is weak since the drift velocity is smaller than the thermal velocity, ($\approx 10^7$ cm/s). It has been found in the same sample that the mobility change is mainly caused by the heating of the photoelectron gas by the electric field.[14] The dependence of T_e on electric field, as obtained from the slope of the high energy tail of the luminescence spectrum, is in good agreement with a simple model using a reasonable value of the energy relaxation time. Shown in panel b of Fig. 5 is the

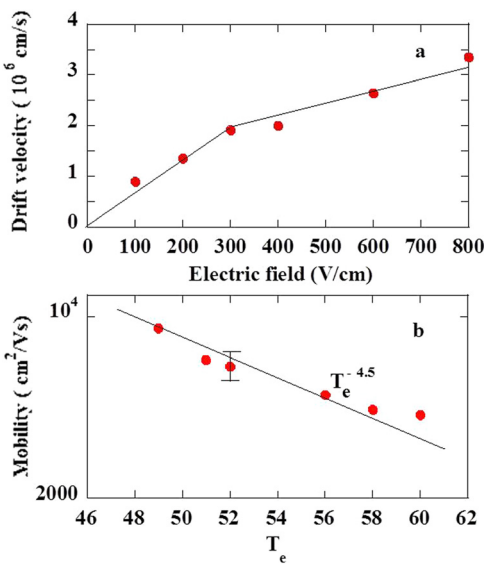

FIG. 5. Panel a shows the electric field dependence of the measured photoelectron drift speed $v = \mu E$. Panel b shows the dependence of the mobility as a function of electronic temperature. One finds a power law of exponent −4.5, similar to the result found elsewhere.[14]

dependence of μ_e as a function of T_e. One observes that the mobility decreases with T_e as a power law of exponent −4.5 that is, very close to that found in Ref. 14.

As seen in Fig. 3 and in the right panel of Fig. 4, the polarization at $r = 0$ strongly increases with the electric field. This is because, in the high electric field regime, such that $\beta L_d \gg 1$ and $\beta L_s \gg 1$, the effective time of residence at the excitation spot (half-width σ) is determined by drift [$\tau_{drift} = \sigma/(\mu E) \approx 10$ ps], which is much smaller than the times for spin relaxation, recombination, and precession (of inverse frequency $\omega^{-1} \approx 10^{-10}$ s/rd). Conversely, at E = 0, the effective spin lifetime at the excitation spot is determined by diffusion ($\tau_{dif} \approx \sigma^2/D \approx 60$ ps) and is comparable with ω^{-1} so that the polarization value is decreased by the Hanle effect.

Once the mobility is known, the charge lifetime τ^* is estimated from the spatial charge profiles using Eq. (4). As seen in the left panel of Fig. 4, the intensity profiles are correctly interpreted by using a value of $\tau^* = 0.33 \pm 0.05$ ns, independent of E. While the uncertainty of this determination, caused by the slight departure of the profile from a Bessel one, masks the possible increase of τ^* with T_e,[28] this value lies in the 0.32–0.40 ns range found for $E = 0$ in the same temperature range using time-resolved luminescence.[3]

We finally interpret the overall shape of the oscillations by adjusting the spin relaxation time T_1 and the polarization loss $\eta \mathscr{P}_i^2$ during thermalization. It is found that, although diffusion during drift induces a nonnegligible damping, the experimentally observed damping is mostly caused by the finite spin lifetime. The value of T_1, shown in Table I, is approximately independent of electric field and is of the order of 0.45 ± 0.1 ns. Again, this value is comparable with the zero-field value of 0.5 ns found elsewhere in the same temperature range.[3] The quantity $\eta \mathscr{P}_i^2$ is estimated from the measured polarization $\mathscr{P}(0)$ at the excitation spot. Its value, also shown in Table I, is smaller than $\mathscr{P}_i^2 = 25\%$, because of polarization losses during thermalization.

The calculated polarization profiles, also shown in the right panel of Fig. 4, correctly interpret the spatial polarization profiles apart from slight discrepancies at small electric field and beyond the first minimum.[29] Table I also gives the value of the spin coherence length $\mu_e E T_1$, defined as the characteristic exponential decay length of the polarization at large distance and for $B = 0$. As expected, this length increases with electric field and reaches a maximum value of 11 μm at high electric field. This result is in agreement with the observation of a maximum in the polarization at a distance of 25μm and after a spin precession angle of 2π, in Curve h of the right panel of Fig. 4.

C. Spectroscopic effects

In this section, we illustrate the ability of the polarized PL imaging technique to investigate spin transport as a function of energy in the emission spectrum. The polarization spectra for $E = 800$ V/cm at increasing distances to the excitation spot are shown in the center and right panels of Fig. 6 for $B = 0.23$ T and $B = 0$ T, respectively. The main effect is that, in agreement with Curves h and h' of the right panel of Fig. 4, the polarization decrease with distance is significantly slower for $B = 0$ T than for $B = 0.23$ T, in which case a change of sign is observed. Note also (i) for all spectra the smaller polarization near 1.49 eV, as interpreted in Sec. II, and (ii) the slightly larger overall polarization at $r = 0$ for $B = 0$ than for $B = 0.23$ T. Since we calculate that polarization losses by precession in the magnetic field give rise are weaker than this difference, this effect is probably caused by spatial inhomogeneities of the sample or rather of the passivating overlayer.[30]

There is a significant difference between the spectra shown in the center and right panels of Fig. 6. Indeed, as shown in the middle panel of Fig. 6, the polarization for $B = 0.23$ T becomes independent of energy in the spectrum at a distance (≈13.5 μm) corresponding to the first

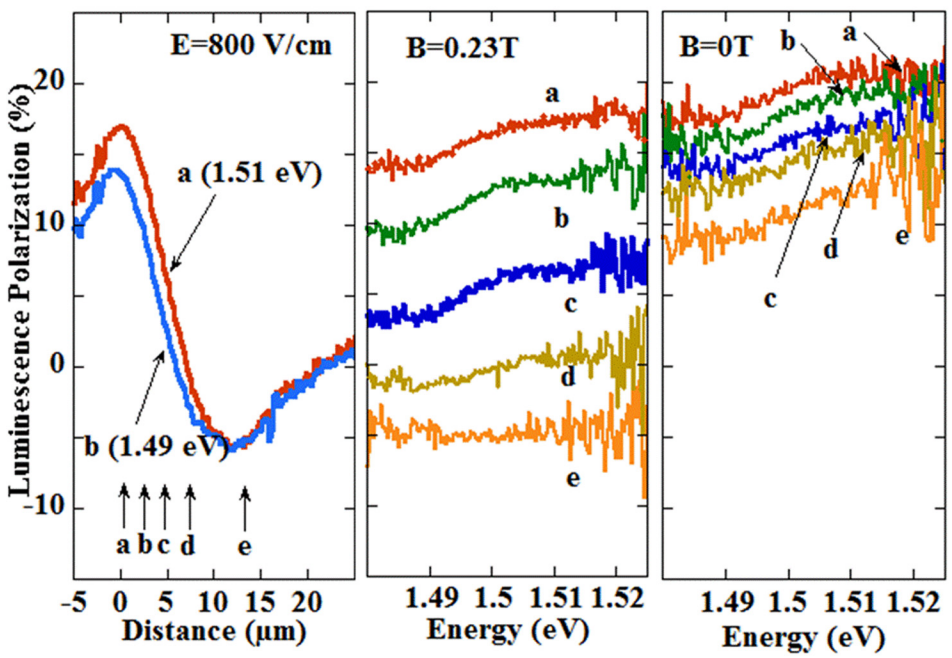

FIG. 6. The left panel shows, for $E = 800$ V/cm, the spatial profile of the polarization at an energy of 1.51 eV (Curve a) and 1.49 eV (Curve b) in the emission spectrum. Slight differences appear up to a distance of 14 μm from the excitation spot corresponding to about the first polarization extremum. The center panel shows luminescence polarization spectra at the excitation spot (Curve a), and at distances, shown by arrows in the left panel, of 2.3 μm (b), 4.6 μm (c), 6.9 μm (d), and 13.8 μm (e). The right panel shows the same spectra as the center panel, but without any magnetic field.

polarization extremum. This effect is also visible in the left panel of Fig. 6, which shows the spatial profiles at the high- and low-energy sides of the spectrum.

We tentatively attribute this spectral effect of the magnetic field to a dependence of the Landé factor on kinetic energy. Semiquantitative verification of this hypothesis uses measurements of the temperature dependence of the g-factor.[31] Taking into account mainly the non parabolicity of the conduction band, it is found that, at a kinetic energy of 20 meV, the g-factor is about −0.32, while it is −0.44 at the bottom of the conduction band. As a result, while electronic spins at the bottom of the conduction band (Curve b of the left panel of Fig. 6) precess by an angle π over a distance of 13.8 μm, the precession angle over the same distance is about $3\pi/4$ for electrons of kinetic energy at $\epsilon = 20$ meV (Curve a). This effect compensates that of the larger luminescence polarization at an energy of 1.51 eV, so that the two curves coincide at the first minimum.

This dependence of spin precession on kinetic energy seems to contradict the assumption that the time for establishment of a thermodynamic equilibrium by e-e collisions is very short, of a fraction of a ps.[32] Here, the time for spin averaging can be estimated experimentally as the drift time until the first extremum, since the polarization oscillations no longer depend on kinetic energy beyond this extremum. This time, of the order of 300 ps, is more than 3 orders of magnitude larger than the momentum relaxation time $\tau_m = \mu m^*/q$. While further investigations must be performed to understand this effect, we think that this strong reduction of the characteristic collision time for spin transport is an effect of the screening of spin exchange collisions by the hole gas, which has been shown to decrease the spin exchange time by several orders of magnitude.[16]

IV. CONCLUSION

We have investigated spin transport in p-type GaAs and have shown that application of an electric field leads to a spin transport over coherence lengths of 11 μm. This has been performed, as described by Fig. 1, by applying a magnetic field in the sample plane and by imaging the polarization spatial profile. Because of spin precession during drift, there appear oscillations in the profile and by monitoring the positions of the extrema, we obtain the photoelectron mobility. This mobility is found to decrease with electric field because of the increase of the photoelectron temperature. It is found that the damping of the oscillations is mostly caused by spin relaxation during drift, which allows us to estimate the spin relaxation time. It is pointed out that the present method may also be used to probe effects of the spin-orbit interaction, in the absence of an applied magnetic field.[33]

ACKNOWLEDGMENTS

The help of A. Wack, D. Lenoir, and P. Njock for mounting the μPL experimental setup and M. Filoche for fruitful discussions is acknowledged. This work was partly supported by the French RENATECH network.

APPENDIX: SOLUTION OF THE DRIFT-DIFFUSION EQUATION

In order to solve Eq. (2) in a semiconducting slab of thickness d, for which the recombination velocity is S for the surface excited by light and S' for the opposite surface, it is first convenient to eliminate the electric field by using $p(r,z) = n(r,z)\exp(\beta x)$, where β is given by Eq. (6) the electric field is along the x direction. The quantity $p(r, z)$ is the solution of the diffusion equation

$$0 = \frac{g(r,z)\tau e^{-\beta x}}{1+\beta^2 L_d^2} - p + \frac{L_d^2}{1+\beta^2 L_d^2}\nabla^2 p. \tag{A1}$$

As shown in Ref. 3, for an arbitrary surface recombination velocity, the solution of this equation is expressed as a sum $\Sigma_m f_m(r)u_m(z)$ of spatial modes, where the functions u_m are eigenfunctions of the Laplacian operator satisfying the boundary conditions defined by the surface recombination velocities at $z = 0$ and $z = d$. The function $f_m(r)$ is a solution of the equation

$$0 = -\frac{f_m(r)}{\tau^*} + \frac{D}{1+\beta^2 L_d^2}\nabla^2 f_m(r) + \frac{e^{-\beta x}}{1+\beta^2 L_d^2}\int_0^d g(r,z)u_m(z)dz. \tag{A2}$$

Here

$$\tau^* = \frac{\tau}{1+\theta_m^2 L_d^2/d^2}, \tag{A3}$$

where θ_m is the solution of $\theta_m = Arctan(\gamma/\theta_m) + Arctan(\gamma'/\theta_m) + (m-1)\pi$ and $\gamma = Sd/D$ and $\gamma' = S'd/D$. The Green function of Eq. (A2) is

$$G(r) = \frac{\tau_{eff}}{2\pi}.K_0\left(\frac{|r_0|}{\mathscr{L}_m}\right), \tag{A4}$$

where

$$\frac{1}{\mathscr{L}_m} = \sqrt{\frac{1}{L_d^2} + \beta^2 + \frac{\theta_m^2}{d^2}}. \tag{A5}$$

The luminescence intensity is taken as $I(r) = A\int_0^d \exp[-\alpha_l z]n(r,z)dz$ where α_l is the absorption coefficient at the luminescence energy and A is a constant. The spatial profile of the luminescence intensity is finally given by

$$I(r) = A\frac{\alpha g_0 \tau e^{\beta x}}{2\pi}\sum_m c_m\left(\frac{\mathscr{L}_m}{L_d}\right)^2\left(K_0\left(\frac{|r|}{\mathscr{L}_m}\right) * e^{\left[-\left(\frac{r}{\sigma}\right)^2+\beta x\right]}\right), \tag{A6}$$

where the symbol * stands for the two-dimensional convolution. In the same way, the spatial profile of the luminescence difference signal, defined as the difference between the components of σ^+ and σ^- helicities, is taken as $I_d(r) = A\mathscr{P}_i\int_0^d \exp[-\alpha_l z]s(r,z)dz$ and given by

$$I_d(r) = A\frac{\alpha g_0 \tau_s \eta \mathscr{P}_i^2 e^{\beta x}}{2\pi} \times \sum_m c_m Re\left\{\left(\frac{\mathscr{L}_m^s}{L_s}\right)^2 \left(K_0\left(\frac{|r|}{\mathscr{L}_m^s}\right) * e^{\left[-\left(\frac{r}{\sigma}\right)^2+\beta x\right]}\right)\right\}, \tag{A7}$$

where the complex length $\mathscr{L}_{ms}$ is given by

$$\frac{1}{\mathscr{L}_{ms}} = \sqrt{\frac{1 \mp iB/\Delta B}{L_s^2} + \beta^2 + \frac{\theta_m^2}{d^2}}. \tag{A8}$$

It has been shown in Ref. 3 that the luminescence profile is dominated by the fundamental mode ($m = 1$), with a marginal contribution of the higher order modes near $r = 0$ for significant surface recombinations. In the same way, using Eqs. (A6) and (A7), we find that the higher order modes weakly affect the positions of the extrema since these extrema lie away from $r = 0$. As a result, in the analysis of the experimental results, it is legitimate to consider only the fundamental spatial mode.

[1]R. Volkl, M. Griesbeck, S. A. Tarasenko, D. Schuh, W. Wegscheider, C. Shuller, and T. Korn, Phys. Rev. B **83**, 241306 (2011).
[2]T. Henn, T. Kiessling, W. Ossau, L. W. Molenkamp, D. Reuter, and A. D. Wieck, Phys. Rev. B **88**, 195202 (2013).
[3]F. Cadiz, P. Barate, D. Paget, D. Grebenkov, J. P. Korb, A. C. H. Rowe, T. Amand, S. Arscott, and E. Peytavit, J. Appl. Phys. **116**, 023711 (2014).
[4]Y. K. Kato, R. C. Myers, A. C. Gossard, and D. D. Awschalom, Nature **427**, 50 (2004).
[5]B. Huang and I. Appelbaum, Phys. Rev. B **82**, 241202(R) (2010).
[6]J. M. Kikkawa and D. D. Awschalom, Nature **397**, 139 (1999).
[7]F. G. G. Hernandez, S. Ullah, G. J. Ferreira, N. M. Kawahala, G. M. Gusev, and A. K. Bakarov, Phys. Rev. B **94**, 045305 (2016).
[8]Z. G. Yu and M. E. Flatté, Phys. Rev. B **66**, 201202(R) (2002).
[9]P. Kotissek, M. Bailleul, M. Sperl, A. Spitzer, D. Schuh, W. Wegscheider, C. H. Back, and G. Bayreuther, Nat. Phys. **3**, 872 (2007).
[10]R. I. Dzhioev, K. V. Kavokin, V. L. Korenev, M. V. Lazarev, B. Y. Meltser, M. N. Stepanova, B. P. Zakharchenya, D. Gammon, and D. S. Katzer, Phys. Rev. B **66**, 245204 (2002).
[11]I. Zutic, J. Fabian, and S. C. Erwin, J. Phys. Condens. Matter **19**, 165219 (2007).
[12]D. Luber, F. Bradley, N. Haegel, M. Talmadge, M. Coleman, and T. Boone, Appl. Phys. Lett. **88**, 163509 (2006).
[13]H. Ito and T. Ishibashi, J. Appl. Phys. **65**, 5197 (1989).
[14]F. Cadiz, D. Paget, A. C. H. Rowe, E. Peytavit, and S. Arscott, Appl. Phys. Lett **106**(9), 092108 (2015).
[15]F. Cadiz, D. Paget, A. C. H. Rowe, and S. Arscott, Phys. Rev. B **92**, 121203(R) (2015).
[16]F. Cadiz, D. Paget, A. C. H. Rowe, T. Amand, P. Barate, and S. Arscott, Phys. Rev. B **91**, 165203 (2015).
[17]I. Favorskiy, D. Vu, E. Peytavit, S. Arscott, D. Paget, and A. C. H. Rowe, Rev. Sci. Instrum. **81**, 103902 (2010).
[18]S. A. Crooker and D. L. Smith, Phys. Rev. Lett. **94**, 236601 (2005).
[19]M. Furis, D. L. Smith, S. Kos, E. S. Garlid, K. S. M. Reddy, C. J. Palmstrom, P. A. Crowell, and S. A. Crooker, New J. Phys. **9**, 347 (2007).
[20]F. Cadiz, D. Paget, A. C. H. Rowe, L. Martinelli, and S. Arscott, Appl. Phys. Lett. **107**, 162101 (2015).
[21]F. M. A. El-Ela and A. Z. Mohammed, J. Mod. Phys. **2**, 1324 (2011).
[22]F. Cadiz, D. Paget, and A. C. H. Rowe, Phys. Rev. Lett. **111**, 246601 (2013).
[23]M. S. Feng, C. S. A. Fang, and H. D. Chen, Mater. Chem. Phys. **42**, 143 (1995).
[24]R. I. Dzhioev, B. P. Zakharchenya, V. G. Fleisher, and V. L. Vekua, Sov. Phys. Semicond. **7**, 1237 (1974).
[25]E. L. Ivchenko and L. V. Takunov, Sov. Phys. Semicond. **10**, 791 (1976).
[26]B. R. Nag, *Theory of Electrical Transport in Semiconductors* (Pergamon, 1972).
[27]R. Ulbrich, Solid State Electron. **21**, 51 (1978).
[28]Since the drift velocity shown in Panel a of Fig. 4 is smaller than the thermal velocity of the photoelectron gas at $T_e = 60$ K by about one order of magnitude, it is considered that the photoelectron statistics are essentially described by the temperature T_e of the photoelectron gas.
[29]These discrepancies may be caused by the presence of a circularly-polarized background of laser light, as can be seen in the sum profiles (see for example, Curve c of the left panel of Fig. 3 for a distance larger than 6 μm.
[30]J. K. Leong, J. McMurray, C. C. Williams, and G. B. Stringfellow, J. Vac. Sci. Technol. B **14**, 3113 (1996).
[31]W. Zawadzki, P. Pfeffer, R. Bratschitsch, Z. Chen, S. T. Cundiff, B. N. Murdin, and C. R. Pidgeon, Phys. Rev. B **78**, 245203 (2008).
[32]W. H. Knox, D. S. Chemla, G. Livescu, J. E. Cuningham, and J. E. Henry, Phys. Rev. Lett. **61**, 1290 (1988).
[33]Here, we calculate that the Dresselhaus spin-orbit interaction, equivalent to a magnetic field of 0.05 T for the maximum electric field value, is too weak to induce observable spatial oscillations of the polarization.